Interfacial instability-driven amorphization/nanocrystallization in a bulk $Ni_{45}Cu_5Ti_{33}Zr_{16}Si_1$ alloy during solidification

Ki Buem Kim,[1] Seonghoon Yi,[2] Haein Choi-Yim,[3] Jayanta Das,[1,4] William L. Johnson,[3] and Jürgen Eckert[1,4]
[1]*FG Physikalische Metallkunde, FB 11 Material- und Geowissenschaften, Technische Universität Darmstadt, Petersenstraße 23, D-64287 Darmstadt, Germany*
[2]*Department of Materials Sciences and Metallurgy, Kyungpook National University, 1370 Sankyuk-dong, Buk-gu, Daegu 702-701, Korea*
[3]*Keck Laboratory of Engineering Materials, California Institute of Technology, Pasadena, California 91125, USA*
[4]*Institut für Metallische Werkstoffe, IFW Dresden, Postfach 270016, D-01171 Dresden, Germany*
(Received 18 July 2005; published 22 September 2005)

We report on experimental evidence for local amorphization/nanocrystallization at the interfaces between the *B*2-ordered Ni(Ti,Zr) phase and the NiTiZr phase with $P6_3/mmc$ during solidification of a multicomponent $Ni_{45}Cu_5Ti_{33}Zr_{16}Si_1$ alloy. So far there are several well-known mechanisms for interfacial amorphization in the solid state but no interfacial instability-driven amorphization/nanocrystallization during transition from liquid to solid state has been reported to our knowledge. The curvature of the interfacial area of the ordered Ni(Ti,Zr) phase is locally negative accompanying reverse atomic diffusion. This results in the frustration of the strong ordering tendency of the Ni(Ti,Zr) phase, and induces local amorphization/nanocrystallization.

DOI: 10.1103/PhysRevB.72.092102 PACS number(s): 64.60.−i, 61.25.Mv, 61.43.Dq, 61.66.Dk

Amorphous phases can be prepared by rapid quenching of melts at cooling rates from 10^3 to 10^7 K/s via bypassing the nucleation of solid phases during solidification.[1,2] On the other hand, it has been found that an amorphous phase can also form from crystalline solids by mechanical alloying,[3] inverse melting,[4] and solid-state interdiffusion reactions of crystalline elements[5] as alternative ways for amorphization. Furthermore, thermodynamic investigations on the transformation from the crystal to the amorphous phase were carried out using molecular dynamics simulations for a binary random solid solution with varying atomic size ratio and concentration, which causes softening of the shear elastic moduli in the supersaturated solid solution.[6] However, the possibility of amorphization driven by an interface instability during solidification has not been investigated by both experiment and simulation so far. Besides basic physical interest in an additional mechanism of amorphization it is also interesting to investigate the structure, the transformation behavior and the thermal stability of an amorphous phase that is driven by an interface instability in order to develop *in situ* bulk metallic glass (BMG) composites, suitable as advanced high-strength materials. BMG composites with a homogeneous *in situ* distribution of nanoscale precipitates[7,8] or ductile dendrites[9,10] have been shown to overcome the limited macroscopic plastic deformability of monolithic BMGs. Among composite-forming alloys, Ni-based BMGs and nanostructured composites can be very attractive for commercial applications due to their high thermal stability,[11] good corrosion resistance,[12] and high strength.[13]

So far there were several trials to form Ni-based BMG composites using typical powder metallurgy methods, such as warm extrusion.[14,15] However, the powder metallurgy production route is rather complicated and expensive compared to conventional casting techniques. Therefore, it is desirable to further develop Ni-based BMGs and nanostructured composites based on the previous investigations on Ni-Zr-Ti-Si BMGs.[16] From these investigations it is interesting to note that the Zr content in the Ni-based alloys is generally much higher than the Ti content. This suggests that Ti is not effective to improve the glass-forming ability of Ni-based alloys. However, it can be a hint for the development of the Ni-based composites instead of monolithic BMGs. Very recently, there was the remarkable finding for a $Ni_{40}Cu_{10}Ti_{33}Zr_{16}Si_1$ alloy to form an extremely stable amorphous phase coexisting with a mixture of crystalline phases.[17] However, there was no detailed report on the amorphization mechanism of such an extremely stable amorphous/crystalline phase mixture during solidification. In this study we investigate the microstructure of an as-cast $Ni_{45}Cu_5Ti_{33}Zr_{16}Si_1$ alloy in detail to suggest the formation mechanism of the amorphous phase upon cooling from the melt.

The multicomponent $Ni_{45}Cu_5Ti_{33}Zr_{16}Si_1$ alloys were prepared by arc-melting a mixture of high-purity elements (>99.9% purity) followed by suction casting. The structural investigation of the sample was performed using x-ray diffraction (XRD, Siemens D500) with Cu $K\alpha$ radiation. Detailed microstructural investigations were performed by high-resolution transmission electron microscopy (HRTEM, Philips CM 20) coupled with energy-dispersive x-ray analysis (EDX, Noran). The TEM samples were prepared by the conventional method of slicing and grinding, followed by ion milling.

Figure 1(a) shows a typical XRD pattern of the as-cast $Ni_{45}Cu_5Ti_{33}Zr_{16}Si_1$ alloy. The dominant diffraction peaks correspond to a CsCl-type phase with *B*2 structure, which can be identified as the NiTi compound.[18] Since the NiTi phase can retain the *B*2 structure also for substitution of Ti by Zr up to 40 at. %,[19] it is feasible to describe the *B*2 NiTi compound as Ni(Ti,Zr) where some of the Ti sites may be occupied by Zr atoms. In addition, there are weak diffraction peaks, which can be identified as NiTiZr and/or Ni_3Ti phases. However, since the NiTiZr and Ni_3Ti phases have the same space group ($P6_3/mmc$) and only a very small difference in lattice parameters,[20] it is very difficult to distinguish

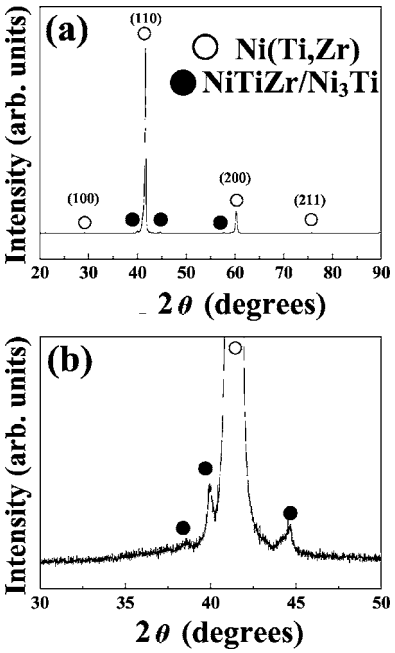

FIG. 1. XRD patterns (a) and (b) of as-cast $Ni_{45}Cu_5Ti_{33}Zr_{16}Si_1$; (b) detailed XRD pattern for 2θ values between 30° and 50°.

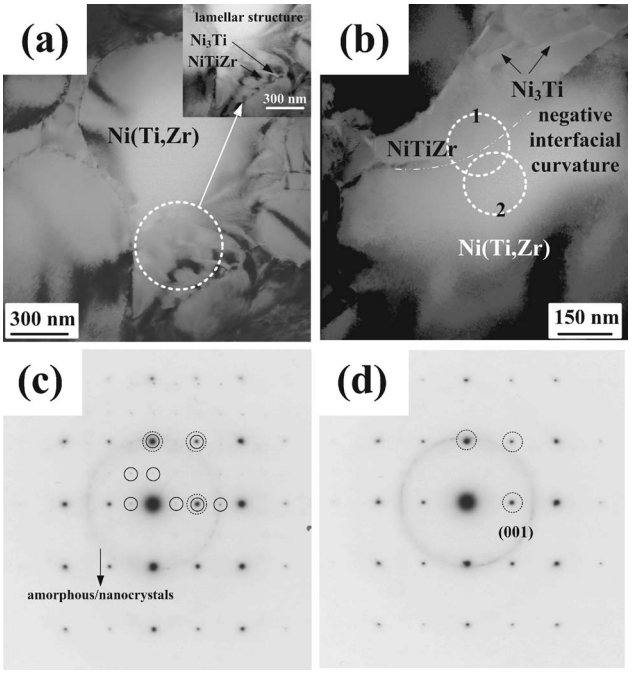

FIG. 2. TEM bright-field images (a) and (b) with a high-magnification bright-field image inset, and selected area diffraction patterns (c) and (d) of as-cast $Ni_{45}Cu_5Ti_{33}Zr_{16}Si_1$; (b) circles 1 and 2 indicate the locations of the selected area aperture; (c) and (d) line and dotted circles indicating the Ni(Ti,Zr) and NiTiZr phases, respectively.

these phases in the XRD pattern. However, a more detailed phase identification of these phases is possible using TEM and EDX (see below) because the NiTiZr and Ni_3Ti phases can be distinguished by chemical analysis. In the range $30° \leqslant 2\theta \leqslant 50°$ the XRD pattern reveals a broad diffraction background [see enlarged XRD pattern in Fig. 1(b)]. This points to a mixture of Ni(Ti,Zr) as the dominant phase, coexisting with the NiTiZr and/or Ni_3Ti phases in the as-cast $Ni_{45}Cu_5Ti_{33}Zr_{16}Si_1$ alloy.

Figure 2 shows TEM bright-field images [(a) and (b)] and selected area diffraction patterns [(c) and (d)] for the as-cast $Ni_{45}Cu_5Ti_{33}Zr_{16}Si_1$ alloy. The overall microstructure [Fig. 2(a)] reveals that spherical grains of 500–1000 nm in size are homogeneously and independently distributed in the matrix. The volume fraction of the spherical grains is approximately 80%. In contrast, the matrix mainly consists of grains of 50–200 nm in size. Furthermore, the microstructure of the matrix is a typical lamellar structure, as indicated in Fig. 2(a), pointing to a eutectic reaction. Therefore, it is feasible to assume that the large and spherical dominant grains form as the primary phase during the solidification.

The details of the microstructure in Fig. 2(b) reveal that the interfacial curvature of the spherical grains is locally negative compared to other interfacial areas between the primary phase and the matrix. As we described above [Figs. 1(a) and 1(b)], the crystalline phases in the matrix can be probably identified using EDX analysis. The crystalline phase with a brighter contrast in the inset of Fig. 2(a) and in Fig. 2(b) exhibits a higher content of Ni ($\sim 57 \pm 3$ at. %) compared to that ($\sim 39 \pm 2$ at. %) for the phase with darker contrast. This suggests that the crystalline phase with the brighter contrast is probably the Ni_3Ti phase, as indicated in Figs. 2(a) and 2(b).

The selected area diffraction (SAD) pattern in Fig. 2(c) was obtained from the interfacial area with negative curvature between the primary Ni(Ti,Zr) and NiTiZr phases, as marked by the circle 1 in Fig. 2(b). This SAD pattern corresponds to a mixture of the [110] and [100] zone axes of Ni(Ti,Zr) and NiTiZr, respectively. The line and dotted circles indicate the diffraction peaks related to Ni(Ti,Zr) and NiTiZr phases, respectively. As marked by line circles in Fig. 2(c), there are diffraction intensities from the (001) superlattice spot of the Ni(Ti,Zr) phase, revealing ordering of this phase. Since these diffraction patterns are strongly overlapped, this points to a good structural coherency between the Ni(Ti,Zr) and NiTiZr phases. Furthermore, there are continuous diffraction rings in Fig. 2(c) with symmetrical spotty diffraction peaks of the Ni(Ti,Zr) and NiTiZr phases.

The selected area diffraction pattern in Fig. 2(d) taken from the edge of the Ni(Ti,Zr) grains near to the negative interfaces between the Ni(Ti,Zr) and NiTiZr phases, as indicated by circle 2 in Fig. 2(b), reveals a continuous diffraction ring with symmetrical spotty diffraction peaks, which can be only identified as the Ni(Ti,Zr) phase. These selected area diffraction patterns indicate that amorphous/nanocrystalline phases form at the edge of the Ni(Ti,Zr) grains. However, it is difficult to observe clear interfaces between the Ni(Ti,Zr) and amorphous/nanocrystalline phases, suggesting that the formation of the amorphous/nanocrystalline phases occurs probably by structural disordering of the Ni(Ti,Zr) phase. Furthermore, it is worth to note that the amorphous/nanocrystalline phase forms at the interfacial area with negative curvature, which should have a different chemical potential in the Ni(Ti,Zr) phase compared to the interfacial area

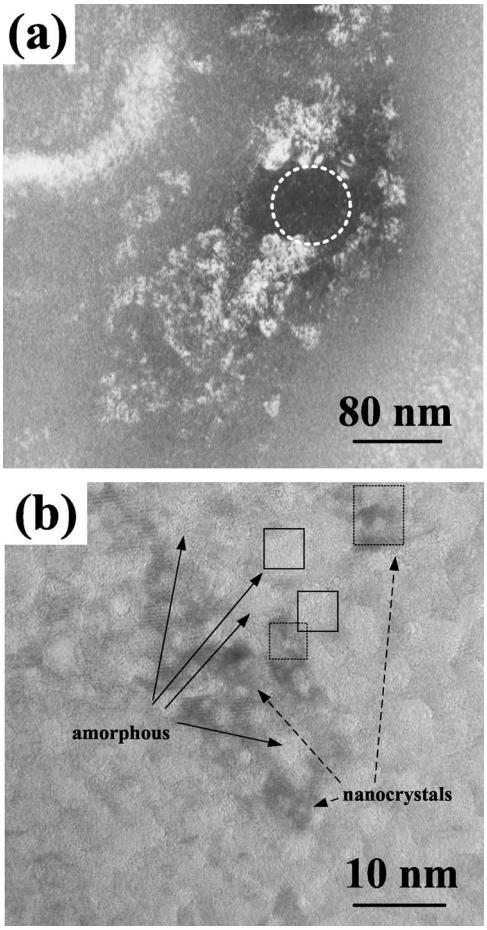

FIG. 3. TEM bright-field image (a) and HRTEM image (b) from the negatively curved interfacial area in as-cast $Ni_{45}Cu_5Ti_{33}Zr_{16}Si_1$. The circle in (a) is the corresponding area for HRTEM in (b). The line and dotted circles in (b) indicate the amorphous and nanocrystalline areas, respectively.

with positive curvature during the growth of the Ni(Ti,Zr) phase due to the effect of the interface curvature on chemical potential of surface atoms. The ordering and multicomponent factors in this alloy can be further effective to change the chemical potential of the surface atoms during solidification. Furthermore, the EDX analysis at the edge of the Ni(Ti,Zr) phase, where the amorphous/nanocrystalline phases form, shows no significant differences in chemistry, compared to that at the central area of the Ni(Ti,Zr) phase. This is probably due to the interaction volume and beam size effects in the EDX analysis.

Figure 3 shows a TEM bright-field image (a) and a HRTEM image (b) from the area to form the amorphous/nanoscrystalline phases, as marked by circle 2 in Fig. 2(b). The bright-field image shows a heterogeneous distribution of nanocrystalline grains of 5–20 nm in size. The central region surrounded by the nanocrystalline phases, as marked by the circle in Fig. 3(a), shows no contrast, which is a typical characteristic of an amorphous phase. However, the HRTEM image from the region without a clear contrast in the bright-field image exhibits a mixture of amorphous and nanocrystalline phases on a very small length scale of less than 10 nm, as indicated by the line and dotted squares for the amorphous and nanocrystalline areas, respectively. This finding also supports that the assumption that the formation of the amorphous phase is very sensitive to the local chemistry at the interfacial areas with negative curvature.

A phase transformation from the crystalline state to an amorphous phase, namely, solid-state amorphization, has been investigated by theoretical consideration of thermodynamics[21,22] and has been supported by experimental results.[4,23–25] This approach involves that unstable supersaturated solid solution phases, such as Ti-Cr (Ref. 4) and Nb-Cr alloys,[23–25] transform to the metastable amorphous phase at the grain boundaries during subsequent heat treatment. This indicates that the grain boundaries of the supersaturated solid solution are locally more unstable than the interior of the grains, thus providing a sufficiently large driving force to nucleate the metastable amorphous phase. Moreover, the thermodymanic model for solid state amorphization at interfaces and grain boundaries concludes that the energy of a crystalline-amorphous interface is lower than that of a crystalline-crystalline interface.[22,26] However, these investigations have been done only using mechanical alloying followed by heat treatment, indicating local solid state amorphization at the interfacial areas.[4,23–25] Therefore, it was unclear whether local interfacial amorphization can also occur under solidification conditions.

In this study, we have observed the formation of amorphous/nanocrystalline phases at the negatively curved interfacial areas of the primary ordered Ni(Ti,Zr) phase during solidification. This type of amorphization is entirely different from the previously reported solid-state amorphization, since it occurs without any subsequent heat treatment directly during solidification. Furthermore, there are no clear interfaces between the primary ordered Ni(Ti,Zr) and amorphous/nanocrystalline phases in the as-cast specimen. This suggests that the formation of amorphous/nanocrystalline phases at the interfacial area is strongly related to an order-disorder transition of the primary Ni(Ti,Zr) phase during solidification. From the kinetic disorder trapping model of Boettinger and Aziz,[27] it is established that the velocity of the growth controls the degree of ordering in intermetallic compounds. From this, it is possible to understand that there can be a significant decrease of the degree of chemical ordering at the interfacial area in the present alloy. Moreover, a transformation of the ordered $NiZr_2$ and NiTi compounds has been demonstrated using molecular dynamics simulation.[28,29] In case of the ordered NiTi phase, the ordered intermetallic compound transforms into an amorphous phase with increasing the lattice instability by either a certain amount of chemical disordering or by a compositional shift from its exact stoichiometry with a range of the Ni content from 15 to 62 at. %.[29] Based on the microstructure and the phase identification presented in Figs. 2(a) and 2(b), it is feasible to suggest a pseudoeutectic reaction by which the Ni(Ti,Zr) phase forms as a primary phase with ejecting the solute into the remaining liquid, followed by the formation of coexisting NiTiZr and Ni_3Ti phases, forming the matrix. Dendritic growth of the primary ordered Ni(Ti,Zr) phase may be very difficult because the growth of this phase seems to be governed by diffusion-controlled kinetic growth.[30] In addition, the growth of the primary or-

dered Ni(Ti,Zr) phase in the $Ni_{45}Cu_5Ti_{33}Zr_{16}Si_1$ alloy can be even more difficult than for the binary NiTi compound due to the multicomponent nature of this alloy, which is expected to frustrate the growth of the crystalline phases.[31] Such complexity of the chemical ordering of the primary Ni(Ti,Zr) phase can be effective to promote the order-disorder transition at the interfacial area of the primary Ni(Ti,Zr) phase. Consequently, there can be different chemical diffusion, i.e., chemical potential, between the ordered and the disordered areas in the Ni(Ti,Zr) phase to eject the solutes into the remaining liquid phase causing an instability of the interface between the primary Ni(Ti,Zr) compound and the remaining liquid. As a result, one can observe a negative curvature of the interfaces between the Ni(Ti,Zr) phase and the matrix. Moreover, a classical solidification model at an off-eutectic composition has pointed out that locally different chemical potentials tend to form a cored structure by an interfacial instability.[32] Therefore, it is reasonable to assume that the local chemical concentration of the solutes will be different according to the curvature of the interfaces of the primary Ni(Ti,Zr) phase, thus stimulating the disordering of the Ni(Ti,Zr) compound in the $Ni_{45}Cu_5Ti_{33}Zr_{16}Si_1$ alloy, and leading to the formation of the amorphous/nanoscrystalline phases at the negatively curved interfacial areas in the present. Such an interfacial instability-driven nanocrystallization has been also observed in a well-known Zr-based bulk metallic glass composites.[33,34]

In summary, amorphization/nanocrystallization driven by an interface instability has been observed in an as-cast $Ni_{45}Cu_5Ti_{33}Zr_{16}Si_1$ alloy during solidification. The amorphization/nanocrystallization occurs at the interfacial area with negative curvature of the interface between the Ni(Ti,Zr) and NiTiZr phases without any clear interface. In contrast the central region of Ni(Ti,Zr) phase is well ordered. This indicates that the occurrence of interfacial amorphization/nanocrystallization in the $Ni_{45}Cu_5Ti_{33}Zr_{16}Si_1$ alloy is strongly related to the negative curvature, causing reverse atomic diffusion to frustrate the ordering tendency of the Ni(Ti,Zr) phase during solidification. These findings are a hint that interfacial instability-driven processes upon solidification may in fact be quite common in complex multicomponent alloys. This opens fascinating perspectives for further investigations and tailoring of phases and microstructures of advanced BMGs and composite materials.

The authors thank F. Baier, G. Miehe, C. Müller, and R. Theissmann for technical assistance and simulating discussions, and U. Kunz for TEM sample preparation. Funding by the EU within the framework of the Research Training Network on ductile bulk metallic glass composites (Grant No. MRTN-CT-2003-504692) is gratefully acknowledged.

[1] W. Klement, R. H. Willens, and P. Duwez, Nature (London) **187**, 869 (1960).
[2] A. Inoue, *Bulk Amorphous Alloys: Preparation and Fundamental Characteristics* (Trans Tech Publications Ltd., Bern, 1998).
[3] C. C. Koch, O. B. Cavin, C. G. McKamey, and J. O. Scarbrough, Appl. Phys. Lett. **43**, 1017 (1983).
[4] Z. H. Yan, T. Klassen, C. Michaelsen, M. Oehring, and R. Bormann, Phys. Rev. B **47**, 8520 (1993).
[5] R. B. Schwarz and W. L. Johnson, Phys. Rev. Lett. **51**, 415 (1983).
[6] M. Li and W. L. Johnson, Phys. Rev. Lett. **70**, 1120 (1993).
[7] G. He, W. Löser, J. Eckert, and L. Schultz, J. Mater. Res. **17**, 3015 (2002).
[8] Y. C. Kim, J. H. Na, J. M. Park, D. H. Kim, J. K. Lee, and W. T. Kim, Appl. Phys. Lett. **83**, 3093 (2003).
[9] C. C. Hays, C. P. Kim, and W. L. Johnson, Phys. Rev. Lett. **84**, 2901 (2000).
[10] U. Kühn, J. Eckert, N. Mattern, and L. Schultz, Appl. Phys. Lett. **80**, 2478 (2002).
[11] M. H. Lee, W. T. Kim, D. H. Kim, and Y. B. Kim, Mater. Sci. Eng., A **375–377**, 336 (2004).
[12] X. Wang, I. Yoshii, A. Inoue, and Y. H. Kim, Mater. Trans., JIM **40**, 1130 (1999).
[13] H. Choi-Yim, D. H. Xu, and W. L. Johnson, Appl. Phys. Lett. **82**, 1030 (2003).
[14] D. H. Bae, M. H. Lee, D. H. Kim, and D. J. Sordelet, Appl. Phys. Lett. **83**, 2312 (2003).
[15] D. H. Bae, M. H. Lee, S. Yi, D. H. Kim, and D. J. Sordelet, J. Non-Cryst. Solids **337**, 15 (2004).
[16] J. K. Lee, D. H. Bae, S. Yi, W. T. Kim, and D. H. Kim, J. Non-Cryst. Solids **333**, 212 (2004).
[17] H. Choi-Yim and W. L. Johnson (unpublished).
[18] PDF#19-0850, PCPDFWIN Version 2.2, JCPDS-International Centre for Diffraction Data, 2001.
[19] PDF#50-1148, PCPDFWIN Version 2.2, JCPDS-International Centre for Diffraction Data, 2001.
[20] P. Villars, A. Prince, and H. Okamoto, *Handbook of Ternary Phase Diagrams* (ASM, Metals Park, OH, 1995), p. 13062.
[21] A. L. Greer, J. Less-Common Met. **140**, 327 (1988).
[22] R. Benedictus, A. Böttger, and E. J. Mittemeijer, Phys. Rev. B **54**, 9109 (1996).
[23] C. Michaelsen, M. Oehring, and R. Bormann, Appl. Phys. Lett. **65**, 318 (1994).
[24] C. Michaelsen, W. Sinkler, Th. Phullmann, and R. Bormann, J. Appl. Phys. **80**, 2156 (1996).
[25] W. Sinkler, C. Michaelsen, and R. Bormann, J. Mater. Res. **12**, 1872 (1997).
[26] M. A. Hollanders, B. J. Thijsse, and E. J. Mittemeijer, Phys. Rev. B **42**, 5481 (1990).
[27] W. J. Boettinger and M. J. Aziz, Acta Metall. **37**, 3379 (1989).
[28] C. Massobrio, V. Pontikis, and G. Martin, Phys. Rev. B **41**, 10486 (1990).
[29] W. S. Lai and B. X. Liu, J. Phys.: Condens. Matter **12**, L53 (2000).
[30] M. Barth, B. Wei, and D. M. Herlach, Mater. Sci. Eng., A **226–228**, 770 (1997).
[31] A. Greer, Nature (London) **366**, 303 (1993).
[32] D. A. Porter and K. E. Eastering, *Phase Transformations in Metals and Alloys*, 2nd ed. (Champman & Hall, London, 1992), p. 231.
[33] U. Kühn, N. Radtke, K. B. Kim, and J. Eckert (unpublished).
[34] K. B. Kim, J. Das, and J. Eckert (unpublished).